Mold Slag Property Measurements to Characterize CC Mold – Shell Gap Phenomena

Y. Meng[1], B.G. Thomas[1], A.A. Polycarpou[1], H. Henein[2] and A. Prasad[2]

1Dept. of Mechanical & Industrial Engineering, University of Illinois at Urbana-Champaign
2Dept. of Chemical & Materials Engineering, University of Alberta, Edmonton, Canada

Keywords: Mold flux, Mold slag, Measurements, Friction coefficient, Viscosity, CCT diagrams, Phase transformations, Glassy – crystalline transition, Steel continuous casting, Gap conduction, Modeling

Abstract

Multi-faceted experiments were conducted to measure the properties of several mold slags, needed for fundamental characterization of heat transfer and friction in the interfacial gap between the shell and mold during the continuous casting of steel. A novel apparatus was used to measure the friction coefficient between solidified mold flux and copper at elevated temperatures. The measured softening temperature is interpreted to extrapolate the slag viscosity-temperature curves far into the low temperature – high viscosity region. Continuous-cooling transformation curves were extracted from XRD analysis of DSC test samples and thermocouple dip tests. Time-temperature transformation curves were obtained from similar analysis of melted mold powder samples that were atomized into droplets, quenched to form glass, and then partially devitrified by reheating to different temperatures for different times and quenched. Polarized light microscopy, SEM, and EDX analysis revealed distinct crystalline and glassy layers, but no severe macro-segregation in a tail-out slag film taken from an operating caster. The results from these new measurements have important implications for the prediction of interfacial gap phenomena, including mold heat transfer, friction, slag layer fracture, and steel surface quality.

Introduction

In the continuous casting of steel, the choice of mold slag is decisive for lubrication and heat transfer control in the mold. The composition, viscosity, solidification temperature and crystallinity are typically considered the most important properties of the slag. These properties determine how the mold powder, which is added to the top surface of molten steel will melt into a liquid layer, (called mold flux or mold slag), infiltrate into the gap between the shell and mold during continuous casting, and there control lubrication behavior, and mold heat transfer. Optimal design of the mold slag can avoid surface defects such as longitudinal, transverse and star cracks; enhance surface quality with the formation of uniform and shallow oscillation marks; prevent breakouts; and enable increased casting speed.

Friction signals can be obtained by installing lubrication sensors[1], load cells[2] or pressure sensors[3] onto the mold to record the mold speed, load or pressure variation during mold oscillation. However, fundamental understanding of the meaning of these measurements and how to interpret them to solve problems is lacking. Currently mold friction measurements are evaluated mainly as a means to detect problems with the oscillation system, such as mold misalignment. If the friction signal can be better understood, then friction monitoring could be used to identify the status of mold lubrication to predict surface defects[1] and to help prevent breakouts[4].

Viscosity of the mold slag is highly temperature dependent. In previous work, the viscosity is often expressed as an Arrhenius-type relationship including the effect of composition [5-7]. These models provide a method to design the slag composition to achieve a desired viscosity curve. However, none of them can accurately predict the viscosity near the solidification temperature. These models are only good for the low viscosity, high temperature range ($<10^3$poise) and cannot accommodate the sharp viscosity increase that occurs at lower temperature. Due to the difficulty of measuring high viscosity, slag viscosity measurements are seldom reported greater than 10Pa·s. Thus, the viscosity-temperature curve near the solidifying temperature is yet unclear for the mold slags used in continuous casting.

Recent laboratory experiments show that heat transfer across the gap is significantly affected by the crystallization of the slag film while it is relatively insensitive to chemical composition [8]. Several studies were conducted using differential thermal analysis (DTA)[9, 10], single or double hot thermocouple technique (SHTT/DHTT)[11, 12], Confocal Microscopy[13] and by devitrification, to measure the fraction of crystalline phase formed after heating a previous quenched sample to a specific temperature and holding[14]. The isothermal transformation diagrams (TTT diagram) and continuous cooling transformation diagrams (CCT diagram) of slag have been determined in controlled laboratory conditions [10, 11, 13, 15, 16]. However, most of

these methods are limited to relatively low cooling rates (1°C/min~900°C/min). The average cooling rate of the mold slag in the longitudinal (meniscus to mod exit) and transverse (mold hot face to steel shell surface) directions may be about 20~25°C/sec, the local cooling rate may be as high as 50~100°C/sec, especially near the meniscus where the maximum heat flux enters the mold. Thus, a method to achieve higher cooling rate is needed to study mold slag crystallization [17]. In this work, several experiments are performed to measure new slag properties, including the friction coefficient between the slag and mold wall, the viscosity at low temperature, the glassy or crystal structure of the solidified flux, CCT and TTT curves, and the crystalline phases.

Experimental

Materials

In this study, four different mold powders were investigated. These are S1 and K1 crystalline slags, S2 glassy slag, and H1 mixed slag-layer film sample taken during tail-out. The chemical compositions of the four powders are listed in Table I. It must be noted that the carbon is added to slow down the mold powder melting and thereby control melting uniformity during the casting process. This carbon burns out during the powder sintering and melting process, so is not generally present in the liquid slag layer or in the re-solidified slag film in the gap. Thus, the powder for slag samples S1 and S2 were prepared without adding the carbon in order to reproduce the actual molten slag in the continuous casting mold without having to experience the experimental difficulties associating with decarburization.

Table I Mold Powder Compositions

	S1	S2	K1	H1
SiO_2	34.33	38.33	31.38	36.01
CaO	29.69	13.30	21.52	35.74
Al_2O_3	5.55	2.43	4.85	4.63
CaF_2	15.93	14.05	28.12	6.82
Na_2O	4.75	13.44	9.57	6.04
MgO	3.05	1.45	0.84	<3.0
TiO_2	<1.0	<0.5	-	<3.0
Fe_2O_3	<1.5	<1.5	0.20	<3.0
MnO	<1.0	<0.5	0.01	<3.0
K_2O	<1.0	<0.5	0.80	<3.0
Li_2O	-	<1.0	-	-
B_2O_3	-	1.41	-	-
C-Total	4.11	11.49	2.36	5.73
CO_2	3.22	3.78	2.75	-
C-Free	3.23	10.46	1.61	

Friction Coefficient Tests

Previous modeling work[18, 19] has shown that the slag properties near the solidification temperature are very important to interfacial lubrication. However, previous measurements focus only on the slag properties at high temperature (greater than 1000°C)[7, 20-24], The lubrication properties of the flux near the softening temperature are rarely reported. Thus, laboratory experiments measuring the friction coefficient of the solid slag layer from room temperature up to 1000°C were conducted.

The prepared relatively carbon free mold powder was melted in a graphite crucible at 1400°C for an hour, and then poured into a preheated metal dish and allowed to air cool. The inner diameter of each sample holder was 20-30mm and the depth was 5mm. The polished sample was then tested in a High Temperature Tribometer (HTT). The HTT is a pin-on-disc tribology apparatus which can measure detailed friction and wear data on test specimens up to 1000°C. The test applies pressure to a 0.25inch diameter steel ball bearing as a top pin that is positioned off-center against a rotating disk sample. The wear track diameter was set to 0.375inch. The spindle velocity was varied from 50rpm to 300rpm. Both the vertical (pressure) and transverse (shear) forces are recorded in order to compute the friction coefficient.

The first series of experiments at room temperature, tested, and increased every 100°C until the machine limit of ~1000°C. It took 3~5 minutes for temperature to reach each set point, which was increased in 100°C intervals. After waiting 5 minutes, data was recorded from the display every two seconds for two minutes, giving 60 data points for each state. To investigate reproducibility and the importance of time in the apparatus, the second series of experiments was conducted by heating to the highest temperature in only 40 minutes and recording data during decreasing temperature intervals using the above recording procedure. Wear track depths were measured with a profilometer which can quantify depth from 0.02mm to 25mm[25].

Time-Temperature Transformation Tests

The onset of crystallization is a strong function of cooling history in slags. Three methods were used to investigate continuous cooling transformation phenomena in slags S1 and S2 over a wide range of cooling rates. A fourth method was used to investigate devitrification during furnace holding after the reheating of previously-quenched samples.

DSC Tests Slags S1 and S2 were analyzed by TG/DSC. Decarbonized mold powder was poured into a platinum micro-crucible. Pure alumina (Al_2O_3) was selected as the reference for all tests conducted. The temperature was increased from room temperature to 1300°C for slag S1 and 1100°C for slag S2 at a heating rate of 10°C/min. These temperatures were sufficient to fully melt each powder. Each sample was then cooled to room temperature at cooling rates of 1°C/min, 5°C/min and 30°C/min in separate tests. The onset temperature of each exothermic peak indicates a crystallization reaction.

Dip Thermocouples To investigate intermediate cooling rates, a series of thermocouple dip tests were conducted. In these tests, a thermocouple, with a bare bead, is dipped into the slag melt in a graphite crucible. It takes a few seconds for the thermocouple to heat up to the slag temperature and reach thermal equilibrium. Then the thermocouple is withdrawn into the air, with a droplet of the slag stuck around the thermocouple bead. The temperature of the thermocouple is continuously recorded by the data acquisition system. By adjusting the initial melt temperature, or by exposing the dip around the thermocouple to different atmospheric conditions, such as forced convection, a range of cooling rates, 0.5°C/sec~50°C/sec, could be achieved.

Atomization (Glass Formation) The real continuous casting process involves rapid initial quenching of the liquid slag against the mold wall followed by slower cooling at different temperatures according to position in the slag layer. To reproduce the high cooling rates, an Impulse Atomization Process (IAP) was used[17]. The mold powder was placed in a graphite crucible and heated in an enclosed tower in a nitrogen atmosphere. At the bottom of the crucible, an array of orifices was machined. By vibrating a plunger inserted into the melt, the molten slag is forced out of the orifices at the bottom of the crucible. The streams disintegrate into droplets according the vibration frequency and fall through the chamber. A mathematical model of droplet solidification was used to predict the cooling history of the droplets[26]. By varying the atomization parameters, particle cooling rates due to the radiation and convection were obtained ranging from 100°C/sec to 13000°C/sec depending on particle size.

Devitrification Tests (Furnace Holding) The atomized material was confirmed to be in a fully glassy state through XRD measurements. This material was then subjected to reheating and furnace holding to investigate devitrification. The amorphous particles were put into a preheated furnace maintained at different temperatures (500°C to 1100°C). After the sample had been held for a set time (1minute to 2hours), it was taken out, and water quenched to room temperature.

Samples Analysis

In order to investigate the evolution of crystallization, all of the slag powder and re-solidified slag samples from continuous cooling and devitrification tests were submitted for X-Ray diffraction (XRD) analysis with Cu K_α radiation to examine the phases present. A piece of film of slag H1 from interfacial steel shell/mold gap was caught as it folded off the mold wall during tail-out after a continuous casting sequence. The slag film was cut into thin slices only 0.03mm thick and mounted on microscope slides. The thin section specimen was then observed under polarized light microscopy in order to distinguish its glassy / crystalline structure. To further investigate the morphology and composition distribution of the slag film, an SEM microstructure analysis was carried out with an energy dispersive x-ray spectroscopy system (EDX).

Results and Discussion

Friction Coefficient

Figure 1(a) gives the results of four friction tests for slag S1. The direction of the arrow on each line shows evolution of temperature during heating or cooling. The friction coefficient varies between runs with an average value 0.16 ± 0.1. Increasing temperature above 800°C causes the friction coefficient to begin to drop. This decrease might correspond to the

oxidation layer formed on the top steel ball bearing pin or alternatively to material softening. In general, there seems to be a slight trend of decreasing friction with increasing temperature which is consistent with a softening phenomenon. However there is lots of variation that can be explained by oxidation. An oxide layer is believed to lubricate the metal/slag interface[27]. Thus, run #7 shows a hysteresis loop with lower friction at later times at the same temperature, which is likely due to oxide layer build-up. The increase of friction just after starting to decrease temperature at the beginning of runs #5 and #8 might be due to spalling of the oxide.

Figure 1(b) shows the friction coefficient as a function of temperature for slag S2. It appears that the friction has a slight drop from room temperature to 500°C. Just above 500°C, the friction coefficient increases sharply from 0.1 to 0.5. This is because the specimen begins to soften. Instead of wear, the ball bearing plows through the tacky slag layer and causes an artificially high increase of friction coefficient. Examination of the sample after the test confirmed that the sample got soft and deformed greatly during the experiment. With increasing temperature, the specimen became too soft to withstand any normal force. After this softening and accompanying deformation, decreasing temperature caused the friction coefficient to fluctuate greatly. This indicates that the surface was too rugged to make any effective measurement, which also happened to a specimen where open bubble holes appeared in the wear track. For the test with slag K1, a similar friction increase with material softening was observed at 720°C. The more gradual increase for this test might be due to the use of a different top pin with a flat surface.

The results show that the friction is relatively insensitive to the microstructure of the slag. It generally stays below 0.2 before softening. The softening of the mold slag, indicated by the apparent dramatic increase in friction coefficient occurs at much lower temperature than previously supposed. This work, for the first time, enables a way to extend the viscosity curves to a lower temperature range.

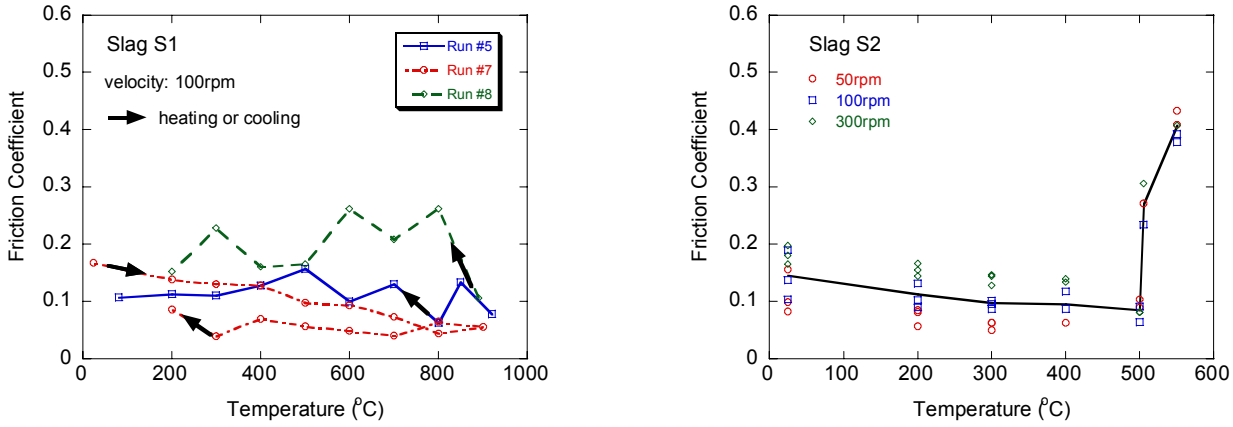

(a) Slag S1 (b) Slag S2

Figure 1: Friction coefficient vs. temperature measured with Tribometer

Viscosity

Viscosity and solidification temperature have been identified as the key physical properties in selecting a mold powder with suitable heat transfer properties. Together with the chemical composition, powder manufacturers commonly measure viscosity at high temperature, as shown in Figure 2. Usually only the low-viscosity part of the curve (<400poise) are measured with a viscometer.

From the high temperature friction test, slags S2 and K1 are known to soften at 500°C and about 720°C, and that slag S1 will likely begin to soften at 1000°C or above. For slag S2, the normal force dropped from 10N to 7N in about one minute while the wear track depression grew to 0.5mm deep. The magnitude of the slag viscosity at the softening point can be estimated roughly from its definition assuming Newtonian flow:

$$\mu = \frac{\tau_{\theta z}}{\dot{\gamma}_{\theta z}} \tag{1}$$

The shear stress, $\tau_{\theta z}$ can be estimated from the recorded friction force, F, and the contact area, A:

$$\tau_{\theta z} = \frac{F}{A} = \frac{F}{\pi r h} = \frac{3.0N}{3.14 \times 3.175mm \times 0.01mm} \approx 30 \times 10^6 Pa \quad (2)$$

Where, r is the radius of the ball bearing, h is the increase in depression depth over one revolution. The strain rate, $\dot{\gamma}_{\theta z}$ can be estimated by assuming $\frac{\partial v_z}{\partial \theta} = 0$:

$$\dot{\gamma}_{\theta z} = \frac{\partial v_\theta}{\partial z} + \frac{1}{r}\frac{\partial v_z}{\partial \theta} = \frac{\partial v_\theta}{\partial z} \approx \frac{\Delta v_\theta}{\Delta z} \approx \frac{25mm/\sec}{5mm} = 5\sec^{-1} \quad (3)$$

Where, Δz is the slag layer total thickness, v_θ is the rotation speed. Combining equations (1)-(3) gives a viscosity of about $6 \times 10^7 Poise$. This value matches with the viscosity of common glass at its softening point[28]. Thus, another point can be added to the viscosity curves. Figure 2 shows estimates of the entire viscosity curves down to the low-temperature high-viscosity (10^8poise) region; the high-temperature low-viscosity (<1000Poise) measured data were supplied by manufacturers. It is interesting to note that inflection(s) occur in the high temperature portion of each curve, perhaps due to partial crystallization.

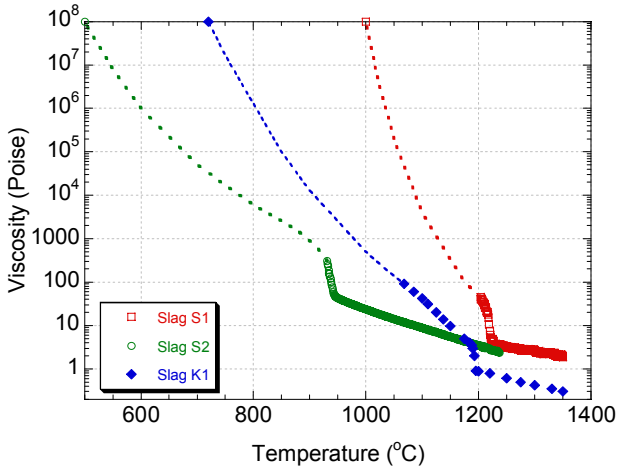

Figure 2: Interpolated viscosity curve

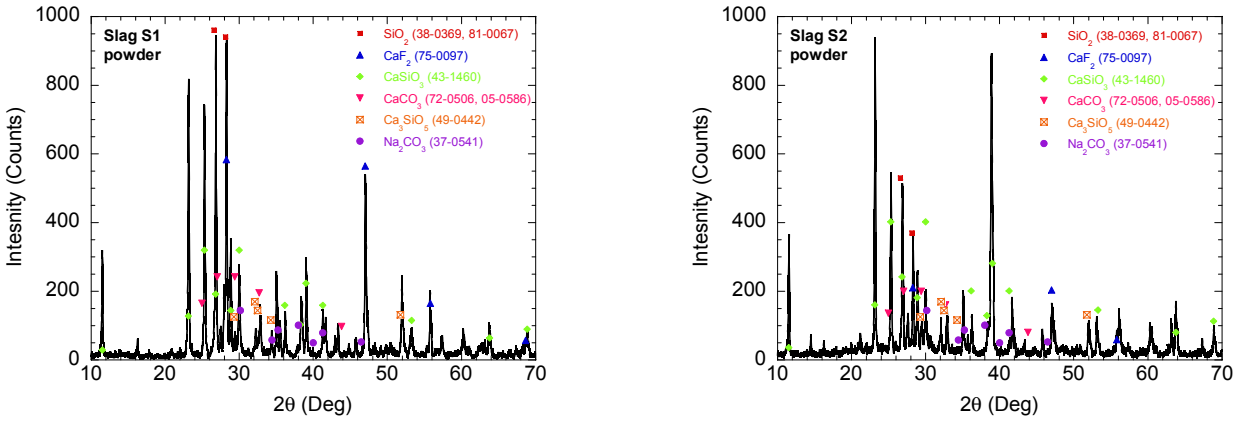

(a) Slag S1 (b) Slag S2

Figure 3: XRD pattern of mold powder

Phase Characterization

XRD analysis was carried out for the initial decarbonized slag powder, re-solidified atomization particles and samples after thermocouple dip tests and furnace holding tests. Figure 3 displays the intensity distribution as a function of diffraction angle of the slag powders before melting, and indicates that the six main phases are: silica (SiO_2), calcium fluoride (CaF_2), wollastonite ($CaSiO_3$), calcite ($CaCO_3$), calcium silicate (Ca_3SiO_5) and sodium carbonate (Na_2CO_3).

The atomized particles had no peaks for crystalline phases, indicating that all droplets of both slags were completely amorphous. The peaks are weaker relative to the background noise for all samples, compared with the slag powder, indicating that the melting and re-solidification produced some glass in every test. Cuspidine ($3CaO•2SiO_2•CaF_2$) is identified in all non-amorphous specimens. The thermocouple dip tests for slag S1 with slower cooling rates indicate calcium silicon oxide fluoride ($SiO_2•2CaF_2$) phase also. This shows that cuspidine crystallizes easily and that perhaps the $Ca_2SiO_2F_4$ crystallization is suppressed by the higher cooling rate.

In slag S1, the first (easiest) phase to form is cuspidine which first appears after holding at 700°C for 30 minutes. With increasing furnace temperature, different phases are found as shown in Figure 4. Nepheline ($Na_2O•Al_2O_3•2SiO_2$) is found in slag S1 at temperatures greater than 900°C. Holding slag S1 longer than one hour at 1100°C causes the peaks of nepheline to disappear and a new phase, gehlenite ($2CaO•2Al_2O_3•SiO_2$) to form, as shown in Figure 4(a).

For slag S2, no crystalline phase forms at 500°C even after two hours of holding. Besides cuspidine, some new phases such as nepheline and calcium silicate ($2CaO•SiO_2$, $8CaO•5SiO_2$) are found in slag S2 when holding at 700°C for two hours. Instead of the gehlenite found in slag S1, a sodium calcium silicate phase ($Na_2O•2CaO•3SiO_2$) is found in slag S2 at 900°C. When the holding temperature is near to the slag melting temperature, only a small amount of crystalline cuspidine phase is observed in the amorphous background (Figure 4(b)). This might due to the lower driving force for crystallization at higher temperature.

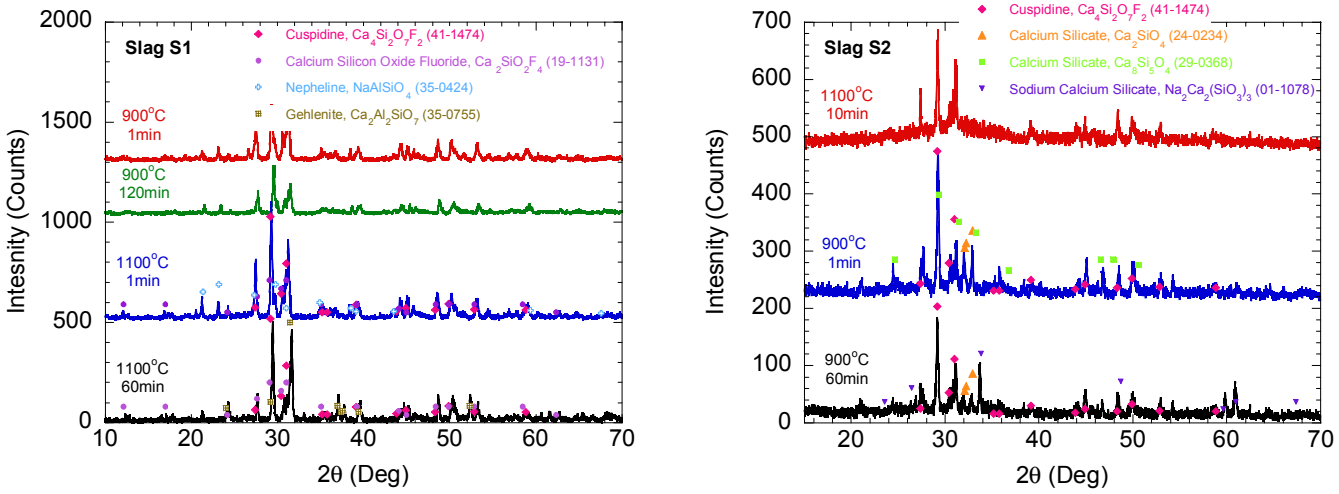

(a) Slag S1 (b) Slag S2

Figure 4: XRD pattern of slag devitrification tests

CCT Curves

Figure 5 shows the DSC curves for slags S1 and S2 generated at a constant heating rate of 10°C/min and cooling rates of 1°C/min. The sharp endothermic trough of the heating curves at 100°C is due to water evaporation. Figure 5(a) also shows two endothermic troughs occurred at around 450°C and 750°C. These troughs are most likely associated with the decomposition of the two common carbonates found in these mold fluxes: Na_2CO_3 at 450°C and $CaCO_3$ at 750°C [29]. This is confirmed by the accompanying weight loss included in Figure 5(a) (TG), which is expected because of the volatilization of CO_2. The series of endothermic peaks above 1000°C on the heating curve indicates that the powder began to melt incongruently. The end of the last peak encountered on heating presumably represents the liquidus temperature. This is seen to be 1235°C for slag S1.

During the cooling process, the phase transformations are very different from heating, owing to the irreversible chemical reactions that occur during melting. Several exothermic peaks were observed, where again phase transformations are indicated. On cooling, the phase transformation is believed to begin at the inflection point starting each peak. For slag S1 at

1°C/min cooling rate, shown in Figure 5(a), the exothermic peaks begin at 1234°C, 1160°C and 1022°C, which might correspond to the onset of three different crystalline phases forming. In general, a higher cooling rate increases the peak height, whereas a lower rate yields higher resolution[30]. Higher cooling rates delay both the onset and finish of each phase transformation.

The results for Slag S2 show a lower liquidus temperature of 1050°C and different exothermic peaks during cooling, as labeled in Figure 5(b). Similar analysis is conducted for different cooling rates and is presented later to construct continuous cooling transformation (CCT) curves.

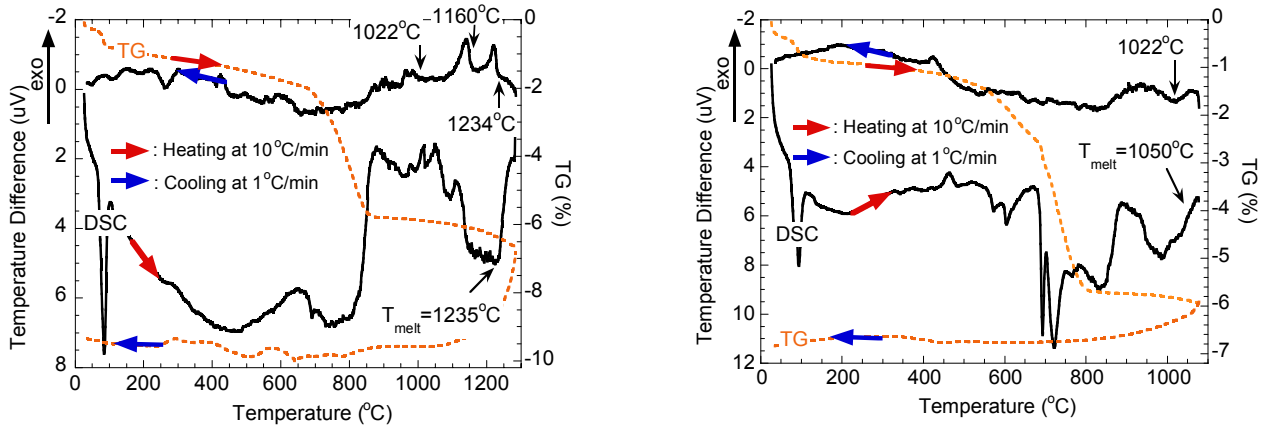

(a) Slag S1 (b) Slag S2

Figure 5: DSC/TG curves at 10°C heating rate and 1°C/min cooling rate

The cooling curves recorded during the thermocouple dip tests were smoothed using the Savitzky-Golay polynomial smoothing filter to eliminate noise. The temperature history curves were numerically differentiated with second order accuracy to distinguish points where the thermal gradient changes would be indicative of crystallization[31]. These points were used for constructing CCT curves.

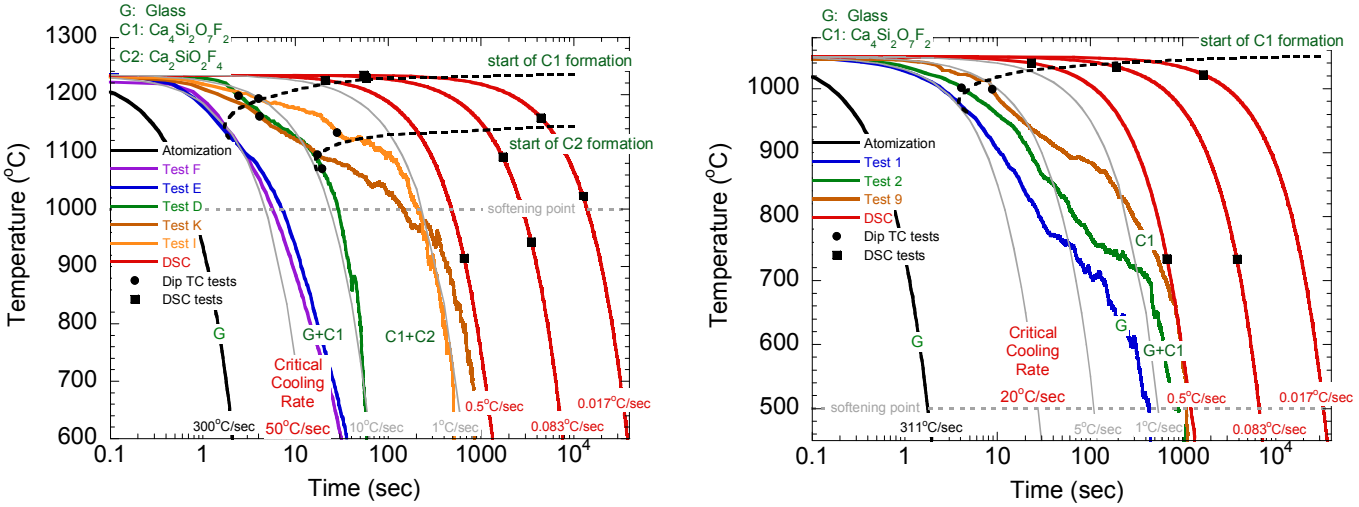

(a) Slag S1 (b) Slag S2

Figure 6: CCT diagrams including the DSC and dip test cooling curves used in their construction

From the time-temperature profiles recorded during the DSC tests and thermocouple dip tests, CCT diagrams were constructed by first taking the time to start at zero when the cooling curves crossed the liquidus temperature (1235°C for slag S1 and 1050°C for slag S2). Figure 6(a) shows the CCT diagram for slag S1. The critical cooling rate to maintain the amorphous structure is estimated to be 50°C/s. At slower cooling rates, the first crystalline phase appears at around 1200°C, which should be cuspidine according to the XRD analysis. Watanabe measured that the liquidus of cuspidine varies between

1114°C (55% CaF_2) and 1407°C (20% CaF_2) in the CaO-SiO_2-CaF_2 ternary system[32]. For slag S1, the liquidus temperature should be ~1250°C, which almost matches with the result in this work. The liquidus temperature of slag S2 is found to be lower. This might be due to the effect of many other compounds in the slag, especially Na_2O, Al_2O_3 etc, which decrease the system melting temperature. When the cooling rate is slower than 10°C/s, a second crystalline phase is formed at around 1100°C, which could be silicon oxide (oxy) fluoride ($Ca_2SiO_2F_4$) phase. The DSC tests with very slow cooling rate (<5°C/min) shows a third peak near 900°C as shown in Figure 5(a). This implies the existence of a third phase which could not be distinguished in the XRD pattern of the thermocouple dip tests. The cooling curves of the dip tests are more ambiguous but do not appear to show the third phase either. This suggests that this phase is suppressed at the faster cooling rate of the dip tests relative to the DSC tests. The XRD results from furnace heating devitrification tests confirm that more crystalline phases form at 900°C to 1100°C. Comparing these results with the phase diagrams[32], these phases generally show lower –temperature liquidus lines which is due to the eutectic reaction.

Similarly, Figure 6(b) shows the CCT diagram for slag S2 and features a critical cooling rate of only 20°C/sec. This low critical cooling rate confirms the conjecture that slag S2 is glassy. The cuspidine phase starts to form at around 1050°C. Other crystalline phases were observed from isothermal aging tests as described in previous section, though they are difficult to distinguish unambiguously in the XRD pattern and cooling curves of thermocouple dip tests.

Slag Film Microstructure

Figure 7(a) shows the different layers and cracks in the slag film H1 under plane polarized light. Figure 7(b) contains the images under cross polarized light. The extinction on the steel side layer proves that it is isotropic. Because crystals of any size or composition have some anisotropic properties, this indicates that the layer closest to the steel is a glassy layer. This suggests that the layer was formed from air quenching the liquid slag while obtaining the sample. Note that the critical cooling rate for obtaining glass is well below typical cooling rates encountered during air cooling, so this finding is reasonable.

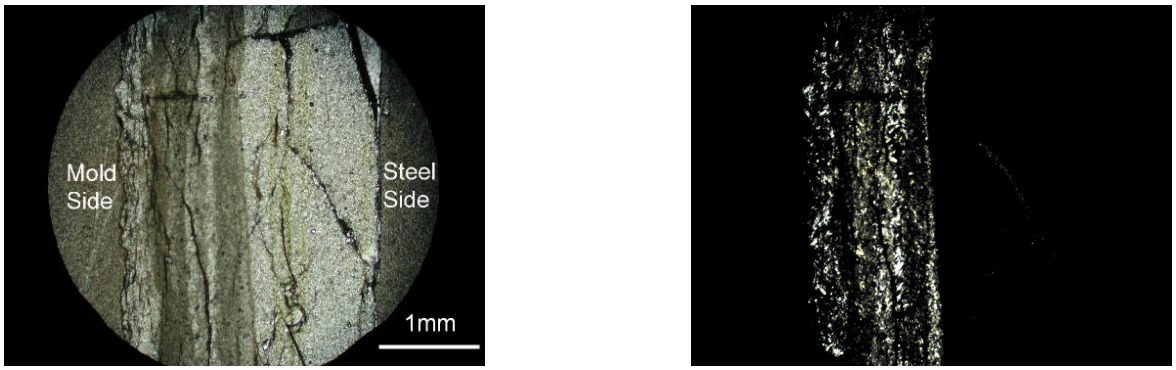

(a) Plane polarized light (b) Cross Polarized light

Figure 7: Polarized light microscopy (slag H1)

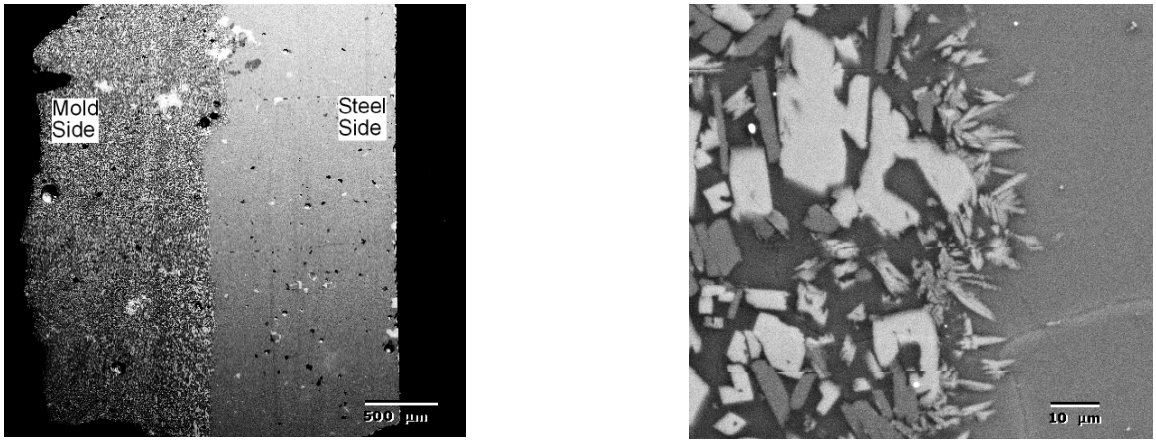

(a) Plane polarized light (b) Cross Polarized light

Figure 8: Polarized light microscopy (slag H1)

Figure 8(a) shows the backscatter electron image (BSE) of the slag H1 film. Figure 8(b) is a close-up of the interface between the two layers. Crystals on the left can be clearly seen growing into the glassy layer on the right. To investigate the composition distribution in the specimen, a series of EDX mappings was performed. Each image was created by mapping the X-ray intensity at each point for a specific element. On the right side (steel side) of each image, all elements are distributed homogenously, which again confirms the glassy microstructure of the right side. The EDX spectrum was also used to identify the element composition of different regions in the sample. The left crystalline side (mold side) is composed of high-calcium grains in a high-silicon background. These likely represent crystals of cuspidine that precipitated. The results indicate that the area average composition is almost the same for the crystal and glassy regions, which indicates that no severe macro-segregation occurred in the gap during casting.

Summary

Experiments are conducted to measure the properties of mold slags which are needed characterize of heat transfer and friction in the interfacial gap between the shell and mold during the continuous casting of steel. These properties include friction coefficient, viscosity at low temperature, CCT curves, TTT curves, and crystal structure composition. Tribometer measurements show that the friction coefficient first decreases slightly with increasing temperature first causes the friction coefficient to slightly decrease with and has an average value of 0.16 ± 0.1. A dramatic rise in friction occurs when the slag begins to soften, which occurs at temperatures as low as 500°C. This softening point allows the slag viscosity – temperature curve to be extended up to 10^8 poise range.

XRD analysis of the mold powders and the samples from DSC tests, and thermocouple dip tests shows that Flourine exists as CaF_2 in pre-melted mold powder and cuspidine is the predominant phase forming in re-solidified slag. The slag crystallization temperatures and products depend greatly on cooling rate. The critical cooling rates are 50°C/sec for crystalline slag S1 and 20°C/sec for glassy slag S2. The main crystalline phases in the re-solidified slag are cuspidine ($Ca_4Si_2O_7F_2$), nepheline ($NaAlSiO_4$), gehlenite ($Ca_2Al_2SiO_7$), calcium silicon oxide fluoride ($Ca_2SiO_2F_4$), calcium silicate (Ca_2SiO_4, $Ca_8Si_5O_{18}$) and sodium calcium silicate ($Na_2Ca_2(SiO_3)_3$). CCT curves for both slags are constructed. Isothermal transformation data was obtained from similar analysis of melted mold powder samples that were atomized into droplets, quenched to form glass, and then partially devitrified by reheating to different temperatures for different times and quenched. Polarized light microscopy, SEM and EDX images show crystalline and glassy layers but no severe macro-segregation in the tail-out slag film taken from an operating caster.

Acknowledgements

The authors would like to thank the Continuous Casting Consortium of the University of Illinois and the National Science Foundation (Grant DMI-01-15486) for financial support. Some analyses are carried out in the Center for Microanalysis of Materials, University of Illinois, which is partially supported by the U.S. Department of Energy under grant DEFG02-91-ER45439. The support of the National Sciences and Engineering Research Council of Canada is also gratefully acknowledged.

Reference

1. B. Mairy, D. Ramelot and M. Dutrieux: "Mold Lubrication and Oscillation Monitoring for Optimizing Continuous Casting", *5th Process Technology Conference: Measurement and Control Instrumentation in the Iron and Steel Industry*, (Detroit, Michigan, USA), ISS/AIME, Warrendale, PA, 1985, pp. 101-17, 134.

2. J.L. Brendzy, I.A. Bakshi, I.V. Samarasekera and J.K. Brimacombe: "Mould--Strand Interaction in CC of Steel Billets. II. Lubrication and Oscillation Mark Formation", *Ironmaking and Steelmaking (UK),* 1993, vol. 20 (1), pp. 63-74, 75.

3. P. Schergen, M. Houbart and R. Heard: "Vibromold, a flexible tool for succcessful high speed casting of sensitive steel grades", *3rd International Metallurgical Conference on CC of Billets*, (Trinec, Czech Republic), Trinecke Zelezarny, Trinec, 739 70, Czech Republic, 1999, pp. 67-77, 111.

4. W.H. Emling and S. Dawson: "Mold Instrumentation for Breakout Detection and Control", *74th Steelmaking Conference*, (Washington, D.C., USA), ISS, Warrendale, PA, 1991, vol. 74, pp. 197-217, 29.

5. P.V. Riboud and M. Larrecq: "Lubrication and Heat Transfer in a Continuous Casting Mold", *Steelmaking Proceedings*, (Detroit, Mich., USA), TMS/AIME, 1979, vol. 62, pp. 78-92, 127, flux viscosity.

6. K. Koyama, Y. Nagano, K. Nagano and T. Nakano: "Design for Chemical and Physical Properties of Continuous Casting Powders", *Nippon Steel Tech. Rep.,* 1987, vol. 34, pp. 41-47, 164, flux viscosity.

7. I.R. Lee, J.W. Kim, J. Choi, O.D. Kwon and Y.K. Shin: "Development of mould powder for high speed continuous casting", *Conference on Continuous Casting of Steel in Developing Countries*, (Beijing, China), Chinese Society of Metals, 1993, pp. 814-22, 170, flux viscosity.

8. R. Taylor and K.C. Mills: "Physical Properties of Casting Powders III: Thermal Conductivities of Casting Powders", *Ironmaking and Steelmaking (UK),* 1988, vol. 15 (4), pp. 187-94, 247, flux thermal conductivity.

9. K. Watanabe, M. Suzuki, K. Murakami, H. Kondo, A. Miyamoto and T. Shiomi: "The effect of mold powder crystallization on heat transfer in continuous casting mold", *NKK Technical Review (Japan),* 1997, vol. 77, pp. 20-26, not labelled.

10. M.S. Bhamra, M.G. Charlesworth, S. Wong, D. Sawyers-Villers and A.W. Cramb: "Crystallization of fluxes under varying cooling rates", *54th Electric Furnace Conference*, (Dallas, Texas, USA), ISS/AIME, Warrendale, PA, 1996, vol. 54, pp. 551-64, 176.

11. Y. Kashiwaya, C.E. Cicutti and A.W. Cramb: "An investigation of the crystallization of a continuous casting mold slag using the single hot thermocouple technique", *ISIJ International (Japan),* 1998, vol. 38 (4), pp. 357-65, 172.

12. C. Orrling, A.W. Cramb, A. Tilliander and Y. Kashiwaya: "Observations of the melting and solidification behavior of mold slags", *Iron and Steelmaker (USA),* 2000, vol. 27 (1), pp. 53-63, 174.

13. C. Orrling, S. Sridhar and A.W. Cramb: "In situ observation of the role of alumina particles on the crystallization behavior of slags", *ISIJ International (Japan),* 2000, vol. 40 (9), pp. 877-85, 173.

14. S. Seetharaman: "Chapter 2: Pertinent Properties for Metals and Slags in Continuous Casting", in *The Making, Shaping and Treationg of Steel 11th Ed.*, vol. Casting, A. Cramb, ed., AISE Steel Foundation, 2003,

15. A.W. Cramb, C. Orrling, Y. Fang, N. Phinichka and S. Sridhar: "Observing and measuring solidification phenomena at high temperatures", *JOM (USA),* 1999, vol. 51 (7), p. 11, 331.

16. K. Tsutsumi, J.I. Ohtake, T. Nagasaka and M. Hino: "Crystallization Behavior of Li2O-SiO2, NA2O-SiO2 and Na2O-CaO-SiO2 Galsses", *Tetsu-to-Hagane (J. Iron Steel Inst. Jpn.),* 1998, vol. 84 (6), pp. 464-69, 363.

17. A. Prasad and H. Henein: "CCT Diagram for Mold Flux Crystallization Studies", *ISSTech 2003*, (Indianapolis, IN), 2003, pp. 257-62, 330.

18. Y. Meng and B.G. Thomas: "Heat Transfer and Solidification Model of Continuous Slab Casting: CON1D", *Metall. Mater. Trans. B (USA),* 2003, vol. 34B (5), pp. 685-705.

19. Y. Meng and B.G. Thomas: "Modeling Transient Slag Layer Phenomena in the Shell/Mold Gap in Continuous Casting of Steel", *Metall. Mater. Trans. B (USA),* 2003, vol. 34B (5), pp. 707-25.

20. M.D. Lanyi and C.J. Rosa: "Casting Fluxes: Physical Properties Affecting Strand Lubrication", *ironmaking and Steelmaking,* 1982, vol. 9 (1), pp. 25-31, 39, flux viscosity.

21. W.L. McCauley and D. Apelian: "Temperature Dependence of the Viscosity of Liquids", *Proceeding of 2nd International Symposium on Metallurgical Slags and Fluxes*, Meallurigical Society of AIME, Warrendale, PA, 1984, pp. 925-47, 219, flux viscosity.

22. K.C. Mills and S. Sridhar: "Viscosities of Ironmaking and Steelmaking Slags", *Ironmaking and Steelmaking (UK),* 1999, vol. 26 (4), pp. 262-68, 148, flux viscosity.

23. P.V. Riboud, Y. Roux, L.D. Lucas and H. Gaye: "Improvement of Continuous Casting Powders", *Fachberichte Huttenpraxis Metallweiterverarbeitung,* 1981, vol. 19 (8), pp. 859-69, 150, flux viscosity.

24. S. Sridhar, K.C. Mills, O.D.C. Afrange, H.P. Lorz and R. Carli: "Break temperatures of mould fluxes and their relevance to continuous casting", *Ironmaking and Steelmaking (UK),* 2000, vol. 27 (3), pp. 238-42, 158, flux viscosity.

25. D.T.K. Lui: *Effect of Oscillation Marks on Heat Transfer in Continuous Casting Molds*, Master Thesis, UIUC, 1995, p.^pp. 1002.

26. A. Prasad, H. Henein and C.A. Gandin: "A Study of Microsegregation in Al-Cu alloys Using Impulse Atomization as an RSP", *Light Metals 2002 Métaux Légers*, (Montreal, Quebec, Canada), 2002, pp. 101-14.

27. H.E. Sliney and C. Dellacorte: "Friction and wear of ceramic/ceramic and ceramic/metal combinations in sliding contact", *Lubrication Engineering,* 1994, vol. 50 (7), pp. 571-76, 378.

28. R.H. Doremus: *Glass Science*, John Wiley & Sons, Inc., New York, 1994.

29. K.C. Mills, A. Olusanya, R. Brooks, R. Morrell and S. Bagha: "Physical Properties of Casting Powders. IV. Physical Properties Relevant to Fluid and Thermal Flow", *ironmaking and Steelmaking,* 1988, vol. 15 (5), pp. 257-64, 364.

30. T. Watanabe, H. Fukuyama, M. Susa and K. Nagata: "Phase diagram cuspidine (3CaO2SiO sub 2 CaF sub 2)-CaF sub 2", *Metallurgical and Materials Transactions B (USA),* 2000, vol. 31B (6), pp. 1273-81B, 356.

31. Y. Meng: *Modeling Interfacial Slag Layer Phenomena In The Shell/Mold Gap In Continuous Casting Of Steel*, PHD Thesis, University of Illinois, 2004.

32. T. Watanabe, H. Fukuyama and K. Nagata: "Stability of cuspidine (3CaO2SiO sub 2 CaF sub 2) and phase relations in the CaOSiO sub 2 CaF sub 2 system", *ISIJ International (Japan),* 2002, vol. 42 (5), pp. 489-97, 360.